Choice of Frequency Ratio and Its Optimization for PWM Inverter Harmonic Distortion Control

M. Shankar*, R.P. Kumudini Devi**

** Electrical and Electronics Engineering Department, Sri Venkateswara College of Engineering, Sriperumbudur, Tamilnadu, India, +919500837386,(email: shankar.auro@gmail.com)*
*** Electrical and Electronics Engineering Department, College of Engineering Guindy, Anna University, Chennai, Tamilnadu, India, +919840002331, (e-mail: rpkdevi@gmail.com)*

Abstract: In this paper, application of numerical-fuzzy logic to choose frequency ratio for pulse width modulated (PWM) inverter is presented. The PWM inverter is a naturally sampled bipolar double-edge modulated. The choice of frequency ratio is based on the total harmonic distortion (THD) and impedance scan of a grid. The THD provides information about harmonic distortion limits. The impedance scan provides information about the harmonic order (H_order) and corresponding principle harmonic voltage (PHV) in utility grid that is to be mitigated. The spectral model of PWM waveform to realize the significance of choice of frequency ratio, harmonic impedance scan procedure of radial grid, and numerical-fuzzy logic applied for choice of frequency ratio are described in detail. The data for numerical-fuzzy controller implemented using MATLAB is obtained from time-domain simulation of the sample system using PSCAD/EMTDC. The individual harmonic distortion profile and instantaneous waveform plot for the choice of frequency ratio using this proposed method demonstrates mitigation of PHV and hence minimization of THD. The Shuffled Frog Leap Algorithm (SFLA) based optimization for the choice of frequency ratio for a global minimum of THD is also presented. Proposed method is also simulated in real-time using Real-Time Digital Simulator (RTDS) and the results presented.

Keywords: Bessel function, sideband harmonics, frequency scan, principle harmonic voltage, carrier harmonics.

1. INTRODUCTION

There is steady growth in renewable energy source integration to low voltage grids (Sandro Gunter et al., 2013). Almost all renewable energy sources (RES) integration to grid is through a frequency converter. The menace of allowable harmonic voltage level breach is a potential threat with increasing distributed generation integration to low voltage grids (Geibel et al., 2012; Shoubaki et al., 2017; Dghim et al., 2018). The RES interfacing converter can participate in distribution grid harmonic control (Tian et al., 2018). So a numerical fuzzy method for choice of frequency ratio of PWM inverter control based on THD measurement and harmonic impedance scan (Dominguez et al., 1994; Hoffmann et al., 2011; Wang et al., 2017) procedure at point of common coupling (PCC) is proposed. This proposed methodology enables mitigation of harmonic distortion in grid-tied wind energy conversion system with battery energy storage. The simulation and real-time results for four different cases are presented. In this proposed method the individual harmonic voltage magnitude (up to 50^{th} harmonics) are measured at PCC. The THD is also computed from individual harmonic voltage values. The grid impedance for different odd order harmonic frequencies (up to 1550Hz) s computed for different scenario of renewable energy source integration to grid using the frequency scan procedure. The harmonic impedance that aggravates parallel/series resonance in AC grid (Sun et al., 2017; Zou et al., 2018) is identified. The choice of frequency ratio for renewable energy source PWM inverter control will be based on the measured THD and harmonic impedance scan data. An artificial intelligence (AI) technique is also proposed to optimize the choice of frequency ratio for a global minimum of THD.

The organization of the paper will be as follows: Section 2 presents the system description and proposed numerical-fuzzy method in detail. Section 3 will present the spectral model of naturally sampled bipolar double-edge modulated PWM waveform in detail. The significance of choice of frequency ratio on degrees of freedom to minimize THD is also presented in this section. The procedure for harmonic impedance scan and related harmonic impedance data of a radial grid under consideration is presented in Section 4. Section 5 will describe numerical-fuzzy controller application to the problem under consideration. The simulation results and discussions are presented in Section 6. The SFLA for optimization of choice of frequency ratio for a global minimum of THD is also presented in Section 7. Section 8 presents RTDS results and Section 9 concludes the paper.

2. PROPOSED METHODOLOGY AND SYSTEM DESCRIPTION

Figure 1 shows the block-diagram representation of sample system that comprises renewable energy source with uncontrolled 3-phase rectifier and battery energy storage system integrated to a radial grid through naturally sampled bipolar double-edge modulated PWM inverter. The grid is modelled as an open loop radial system with three nodes. The renewable energy source is connected at node-2 of the grid. The frequency ratio of the PWM inverter controller is varied in odd multiples of three and the corresponding individual harmonic and THD data are measured at the node of interest. The harmonic impedance scan is also performed at the renewable energy source integration point to get the information about the H_order and corresponding PHV.

Figure 2 shows the methodology for choice of frequency ratio implemented in MATLAB fuzzy logic tool box. The principle harmonic voltage (PHV) which is to be mitigated is correlated with the individual harmonic and THD data. The frequency ratio that facilitates minimum THD is of choice. More than one frequency ratios can fulfill this constraint. In such event, the individual harmonics for these frequency ratios are correlated with PHV of impedance scan data. The frequency ratio which has more individual harmonics around PHV is discarded from choice. Thereby a choice of frequency ratio is arrived and is fed to the controller of the PWM inverter.1

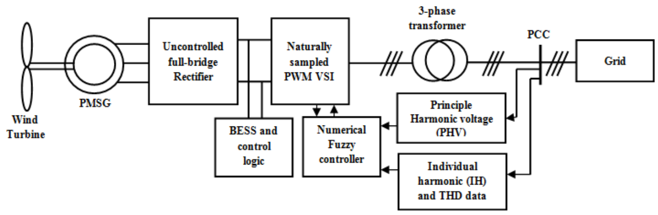

Fig. 1. Sample system.

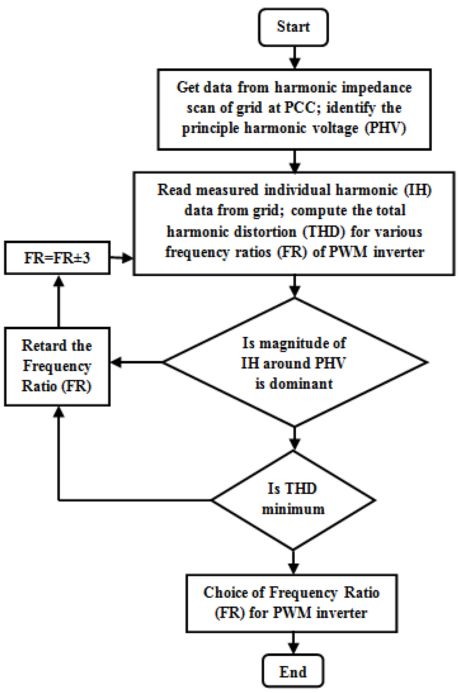

Fig. 2. The methodology proposed for choice of frequency ratio based on THD and impedance scan at PCC implemented in Fuzzy logic.

3. SPECTRAL MODEL OF PWM WAVEFORM

The spectral model of bipolar double-edge modulated PWM waveform of DC-AC converter using double Fourier series method (Vasca.F, 2012) is given by:

$$SM_{bpdpwm}(t) = \frac{M}{2}\cos(\omega_1 t + \theta_1) + \sum_{m=1}^{+\infty} \frac{2}{m\pi} J_0\left(\frac{m\pi M}{2}\right) \sin\frac{m\pi}{2} \cos[m(\omega_c t + \theta_c)] + \sum_{m=1}^{+\infty} \sum_{n=\pm1}^{\pm\infty} \frac{2}{m\pi} J_n\left(\frac{m\pi M}{2}\right) \sin\frac{(m+n)\pi}{2} \cos[m(\omega_c t + \theta_c) + n(\omega_1 t + \theta_1)] \quad (1)$$

where $M = \dfrac{2R_1}{C_m}$ is the index of modulation, R_1 the reference signal maximum magnitude and C_m the magnitude of carrier signal measured peak-peak.

ω_c and ω_1 are the carrier and reference signal angular frequencies respectively.

θ_c and θ_1 are the carrier and reference signal initial phase angles respectively.

$J_n\left(\dfrac{m\pi M}{2}\right)$, is the Bessel function of kind one.

The prime term in (1) is the fundamental output, followed by carrier frequency harmonics term and finally the sideband terms of the carrier signal and its harmonics. Many waveforms will be present in the PWM waveforms which are the cluster of carrier frequencies and associated harmonics, whose frequency will be $f = mf_c, m = 1,2,....,+\infty$ and $f = mf_c + nf_1, n = \pm1,\pm2,....,\pm\infty$ is the frequency of the sideband harmonics whose amplitude is given by:

$$J_n\left(\frac{m\pi M}{2}\right) \quad (2)$$

For order $n = 0$, the Bessel functions connive is shown in Figure 3. Figure 4 illustrates connive for Bessel functions of order $n = 1,2,3$. These connives illustrate the basic distinctiveness of Bessel functions. It is evident that the sideband harmonics typically materialize in duo and are symmetrical about each carrier harmonics, which is its nature. The Bessel functions describe the magnitude of the carrier and sidebands. They also characterize the magnitude, and thus attenuation, of the modulating signal and generation of harmonics of that signal. Looking into the sideband magnitude of the equation, if is even, In the case of double-edge modulation, if $(m+n)$ term in sideband magnitude of (1) is even, all sideband and carrier harmonics of even-order and odd-order are nullified.

An inverter which is used for renewable energy source in power systems is supposed to be free from even harmonics which enables any existing asymmetry in phase-phase voltage to be eliminated. So a decisive factor in the choice of modulation principle is the frequency ratio, p of the modulation frequency, f_c to the output frequency, f_1:

$$p = \frac{f_c}{f_1} \quad (3)$$

This factor establishes the harmonic spectrum for an assured degree of control for a given modulation pattern. An adequately hefty value of this ratio will minimize all the low-order harmonics to be well within specified limits. However, a high-frequency ratio will yield switching losses of significant value which has to be also well within limits to ensure efficient operation of PWM inverter.

The fundamental and harmonic voltages can be controlled simultaneously by reversing the phase potentials a number of times in each half-cycle at predestined angles of the square wave. For the given fundamental switching frequency every reversal grants one degree of freedom. This degree of freedom allows either cancelling a harmonic component or controlling the magnitude of the fundamental voltage. Thus for k reversal per half-cycle one reversal is utilized for controlling the fundamental voltage magnitude. Remaining $(k-1)$ degrees of freedom is used to reduce $(k-1)$ individual low-order harmonics or to minimize the THD. This $(k-1)$ degrees of freedom is a function of the carrier frequency. This proposed methodology utilizes this degree of freedom to minimize the THD by optimally selecting the carrier frequency based on THD and impedance scan of the grid. Figure 5 shows possibilities of varying the degrees of freedom for different carrier frequency.

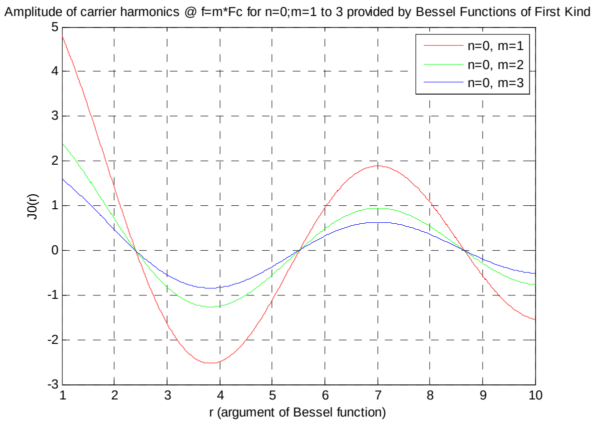

Fig. 3. Magnitude of carrier harmonics provided by Bessel functions of First kind of integer order.

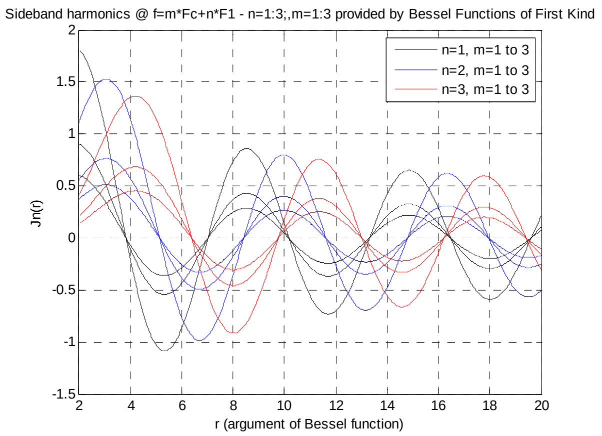

Fig. 4. Magnitude of sideband harmonics provided by Bessel functions of First kind of integer order.

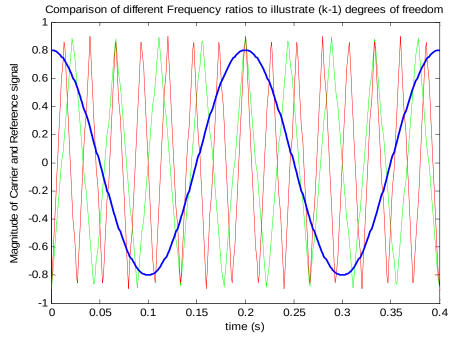

Fig. 5. Comparison of Frequency ratios to illustrate utilization of $(k-1)$ degrees of freedom.

4. HARMONIC IMPEDANCE SCAN

The concept of active filtering evolves as the inverters connected to grid can inject harmonic currents to compensate for the PHV of grid. In the PWM control of all the inverters connected to grid if it is facilitated to enable control based on PHV and harmonic grid impedance, the inverters could then feed in the current that is required to compensate these voltages (Arricibita et al., 2017). The grid harmonic impedance changes following the dynamics of power system components with time (Henrique et al., 2017). So a need arises to predict a schedule for the inverter to inject harmonic currents to compensate for PHV. To prepare the schedule, grid harmonic impedance is to be measured with sequence impedance model of power system (Vieto and Sun, 2018). In this proposed methodology, the knowledge of grid harmonic impedance facilitates choice of frequency ratio that eliminates PHV.

The first step in assessing the grid harmonic impedance is to perform the frequency scan of harmonic model of the power system under consideration. Literature (Task force on Harmonics Modeling and Simulation, 1996 a, b) documents in detail the harmonic modeling of various power system components. Then the solution of network equation (4) for each harmonics will be arrived.

$$\left[I_m\right]=\left[Y_m\right]\left[V_m\right];m=1,2,3,...,n \tag{4}$$

The term $\left[Y_m\right]$ is the admittance matrix of the system under consideration. $\left[I_m\right]$ the source current matrix and $\left[V_m\right]$ the matrix of bus voltages. The elements of the matrices are for harmonic number, m .

In the PSCAD/EMTDC frequency scan procedure (Dennis Woodford, 2017), the basic principle is, at the PCC a one per unit magnitude of current at odd order harmonics up to 1550Hz is injected. Then Equation (4) is solved for the PCC voltage by setting the other currents to zero. Now the voltage that is obtained is equal to the driving-point impedance looking into PCC. In this work the PCC is where the RES is integrated to the grid (node-2) through a PWM inverter. This procedure presents the impedance levels and significant voltage distortions at PCC.

The analysis is performed for harmonic frequency range from 50Hz to 1550Hz in steps of odd multiples 50Hz. The results of harmonic impedance scan procedure are the impedance levels and potential voltage distortion at PCC. These data facilitates identification of the series and parallel resonances (PHV) in the network. Table 1 presents the impedance scan results at PCC. Figure 6 shows the plot of PCC positive sequence impedance scan data.

Table 1. Impedance scan result at PCC.

F(Hz)	|Z+|(ohms)	PHASE(Z+)(Deg)
50	2.191972865	74.54533092
150	7.943765452	64.12718428
250	18.35925354	24.90771424
350	17.35918244	-33.79456299
450	11.26307221	-57.85232128
550	8.178614302	-67.43227771
650	6.453657618	-72.44332918
750	5.355396134	-75.54029729
850	4.59148318	-77.65908935
950	4.026909939	-79.20878561
1050	3.591132945	-80.39653457
1150	3.24367914	-81.33878234
1250	2.959611084	-82.10625206
1350	2.722684999	-82.74452244
1450	2.521840384	-83.284374
1550	2.349269546	-83.7473943

5. NUMERICAL-FUZZY CONTROLLER

Most of the real-world controls are performed based on the numerical data obtained from sensing elements and linguistic expertise form human. A fuzzy rule base that combines the numerical and linguistic expertise presented in literature (Li-Xin and Jerry Mendal, 1992) is applied in this proposed method to choose frequency ratio for PWM inverter. The inputs to the numerical-fuzzy controller are the data from harmonic impedance scan procedure, the individual harmonic voltage measured and THD calculated at PCC. The output will be frequency ratio choice for PWM inverter. The inputs and output are divided into fuzzy regions and each region is assigned with a fuzzy membership function as in Table 2.

The fuzzy rules are generated from human expertise on correlation of individual harmonic data with the principle harmonic voltage (PHV) data for a sequence of harmonics order.

If individual harmonic voltage pertaining to a harmonic order around principle harmonic voltage is high, the constraint minimum PHV ($min(\text{PHV})$) is not fulfilled and the rule is weighted low. If the constraint is fulfilled, the rule is weighted high. The other constraint is minimum THD ($min(\text{THD})$). The choice of frequency ratio (FR) output is correlated with fulfillment of both constraints. Based on the results of harmonic impedance scan, individual harmonic and THD measurements at PCC, the input-output fuzzy regions and associated membership functions are as given in Table 2. For simulation purpose the rule base is framed with 60 rules. Figure 7 presents the fuzzy rule viewer. The surface view of the rule base is shown in Figure 8.

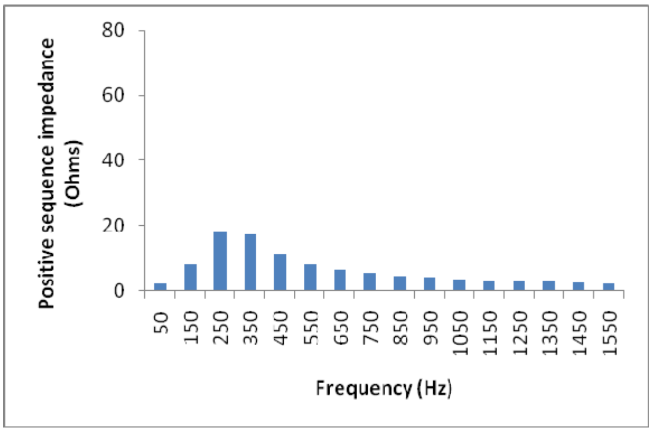

Fig. 6. Plot of positive sequence harmonic impedance scan result of PSCAD/EMTDC simulation.

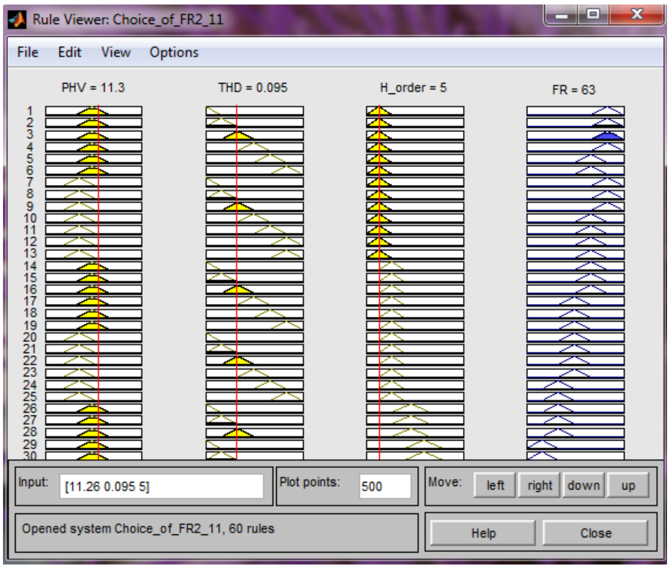

Fig. 7. Fuzzy rule viewer.

For any given input data set, the controller provides the choice of frequency ratio for PWM inverter. Figure 9 shows the simulation diagram that outputs choice of frequency ratio for given input data.

Table 2. Input-output fuzzy regions and assigned fuzzy membership function.

Division of Input-Output numerical data into fuzzy regions	Input-1: H_order data		Input-2: PHV data		Input-3: THD data		Output: FR data	
	Start of MF region	End of MF region	Start of MF region	End of MF region	Start of MF region	End of MF region	Start of MF region	End of MF region
Extremely Small (ES)	--	--	2	3.28	0.0	0.05	--	--
Very Small (VS)	1	9	2.7	4.05	0.0	0.1	18	36
Small (S)	5	13	3.28	4.95	0.05	0.15	27	45
M (Middle)	9	21	4.05	7.37	0.1	0.2	36	54
Large (L)	13	25	4.95	10.81	0.15	0.25	45	63
Very Large (VL)	19	31	7.37	13.27	0.2	0.3	54	72
Extremely Large (EL)	--	--	10.81	19	0.25	0.3	--	--

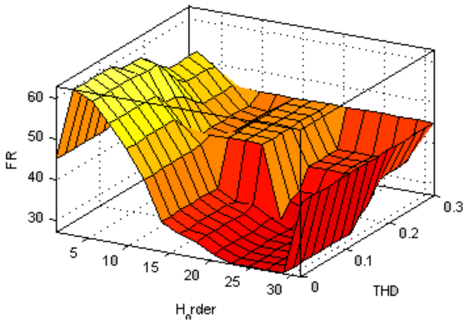

(a)

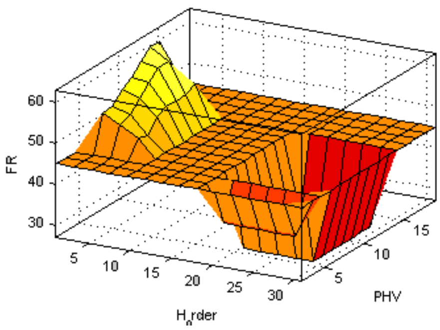

(b)

Fig. 8. Surface view of rule-base with (a) H-order & THD (b) H-order & PHV as inputs and FR as output.

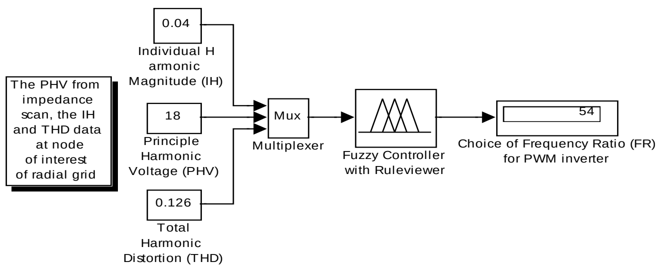

Fig. 9. Simulation diagram that outputs choice of frequency ratio for given input data.

6. RESULTS AND DISCUSSIONS

The sample system comprises a wind turbine generator integrated to a radial grid at node-2 through an uncontrolled three phase full bridge rectifier and PWM voltage source inverter (WECS). A battery energy storage (BES) model is connected to the DC bus through a DC-DC buck-boost converter to enable voltage stability as the wind energy is variable most of the time. As discussed in section 2, in this proposed methodology to enable choice of frequency ratio for PWM control, first the impedance scan is performed at the node-2 where the renewable energy source is integrated. From the positive sequence impedance result obtained from impedance scan procedure described in section 4, given in Table 1, it is evident that the PHVs are the 5th harmonic and around. So, in developing the fuzzy rule base, up to 15th order harmonics alone are considered. These results (PHVs and corresponding harmonic order) are one of the inputs to numerical-fuzzy inference.

The individual harmonic (IH) voltages measured and THD calculated at node-2 for different frequency ratios of the PWM inverter are the other two inputs to the fuzzy-inference. As per IEEE Std 519 – 2014 IEEE Recommended Practice and Requirements for Harmonic Control in Electric Power Systems clause 3 Definitions for THD, the THD is to be computed including first 50 harmonics and even higher if required. In this work, in developing the fuzzy switching frequency control algorithm, odd order harmonics up to 49th harmonic measured at PCC is considered for calculating the THD. The measured result for frequency ratios $p = 33, 45, 57 \; and \; 63$ is presented in Table 3. For the frequency ratio of 33 and 45 the THD is high comparably. So these frequency ratios are discarded as one of the constraints is $min(\mathrm{THD})$. For frequency ratios of 57 and 63, the THD is low and are also approximately equal. In order to fulfill the other constraint $min(\mathrm{PHV})$, the harmonic impedance data and individual harmonic distortion data are correlated. For frequency ratio of 63, the individual harmonic voltage dominant is in correlation with the PHV and hence choice of this frequency ratio is discarded. Both the constraints are fulfilled by the frequency ratio 57 which is the output of numerical-fuzzy inference for PWM inverter control.

In order to prove the proposed fuzzy frequency control algorithm, simulations are performed for four different cases. First three cases are for functions of harmonics at WECS source end and the fourth case is at load end. Case 1, 2 and 3 are, without BES (WoB) in the DC bus, with BES without its thermodynamics effect (WBwoeT), with BES with its thermodynamics effect (WBweT) (Shankar and Kumudini

Devi, 2016) and case 4 is injection of harmonic current (H-inj) at node-3 of grid. For all these cases, the individual harmonics is measured and THD calculated at PCC up to 63rd harmonic. Table 4 presents the simulation results in terms of IH and THD for conventional case with frequency ratio 33. Figure 10 shows the IH plot of conventional method for different cases.

Table 3. IH voltages and THD data for frequency ratios $p = 33, 45, 57$ and 63.

H_order	Harmonic voltage magnitude for different frequency ratios			
	p = 33	p = 45	p = 57	p = 63
1	0.9536	0.9776	0.9867	0.9926
3	0.02	0.0122	0.0231	0.0097
5	0.03	0.0283	0.0241	0.0095
7	0.03	0.0147	0.0237	0.0858
9	0.01	0.0018	0.0279	0.0063
11	0.01	0.0122	0.0146	0.0054
13	0.01	0.0314	0.0213	0.0014
15	0.01	0.0392	0.0121	0.0557
17	0.0035	0.0209	0.0032	0.0199
19	0.009	0.023	0.0226	0.0056
21	0.015	0.0291	0.0168	0.0014
23	0.0125	0.0104	0.0361	0.0172
25	0.01	0.0267	0.0557	0.0204
27	0.022	0.0261	0.0173	0.0071
29	0.042	0.0403	0.0229	0.0045
31	0.168	0.0107	0.0115	0.0104
33	0.02	0.0094	0.0329	0.0059
35	0.145	0.0075	0.0274	0.0065
37	0.03	0.0092	0.0062	0.0057
39	0.009	0.0012	0.0046	0.0136
41	0.0055	0.0346	0.0093	0.0047
43	0.006	0.0905	0.0021	0.0024
45	0.009	0.0065	0.0102	0.0065
47	0.004	0.059	0.0058	0.0106
49	0.0025	0.0104	0.0048	0.0008
THD	**0.2486**	**0.1522**	**0.1090**	**0.1127**

The results show that for all the cases, the IH is dominant for frequency ratios 35 and 37 which are around 33. From THD results, it is evident that the THD is 0.27pu for WoB case which is comparatively large against 0.24pu for WBwoeT case.

Table 5 presents the results of proposed fuzzy method whose output frequency ratio is 57. Figure 11 shows the IH plot for proposed method for different cases. The results show that for all the cases, the IH is not dominant for any frequency ratio. The results also show that the THD is around 0.1pu for source end (WoB, WBweT and WBwoeT) voltage harmonic influence cases and 0.07pu for load end (H_inj) case.

Table 4. IH voltages and THD results for different cases with conventional control (p = 33).

H_order	Harmonic voltage magnitude for different cases ($p = 33$)			
	WBweT	WBwoeT	WoB	H_inj
1	0.964	0.9536	0.9784	0.9196
3	0.03	0.02	0.0125	0.0069
5	0.03	0.03	0.0291	0.0246
7	0.032	0.03	0.0167	0.0091
9	0.015	0.01	0.0118	0.0097
11	0.004	0.01	0.0123	0.0094
13	0.017	0.01	0.013	0.0147
15	0.016	0.01	0.011	0.006
17	0.008	0.0035	0.0085	0.0036
19	0.002	0.009	0.0067	0.0037
21	0.015	0.015	0.011	0.0104
23	0.015	0.0125	0.016	0.0074
25	0.005	0.01	0.0054	0.0149
27	0.03	0.022	0.0065	0.0082
29	0.043	0.042	0.04	0.0418
31	0.1782	0.168	0.1941	0.1718
33	0.023	0.02	0.02	0.0284
35	0.153	0.145	0.165	0.1433
37	0.033	0.03	0.0277	0.0191
39	0.013	0.009	0.021	0.011
41	0.004	0.0055	0.009	0.004
43	0.011	0.006	0.0083	0.0093
45	0.01	0.009	0.0035	0.004
47	0.003	0.004	0.0045	0.0052
49	0.0036	0.0025	0.0024	0.002
51	0.0036	0.0045	0.0026	0.002
53	0.0021	0.0012	0.0017	0.0013
55	0.001	0.0007	0.0005	0.0011
57	0.0012	0.0006	0.0008	0.0011
59	0.001	0.00002	0.0011	0.0014
61	0.002	0.0025	0.0002	0.0017
63	0.0011	0.0011	0.0002	0.0029
THD	**0.262713**	**0.248715**	**0.271834**	**0.254815**

Table 5. IH voltages and THD results for different cases with proposed fuzzy method

H_order	Harmonic voltage magnitude for different cases with proposed method			
	WBweT	WBwoeT	WoB	H_inj
1	0.9955	1.001	0.9744	0.9925
3	0.014	0.008	0.0188	0.011
5	0.014	0.011	0.0194	0.0182
7	0.035	0.015	0.0315	0.007
9	0.015	0.015	0.0199	0.0133
11	0.0055	0.016	0.0033	0.0144
13	0.0088	0.012	0.0051	0.0058
15	0.0058	0.0055	0.0058	0.0098
17	0.011	0.0065	0.0105	0.0065
19	0.0155	0.019	0.013	0.0051
21	0.025	0.03	0.019	0.0187
23	0.026	0.024	0.019	0.027
25	0.049	0.039	0.049	0.004
27	0.0135	0.01	0.012	0.016
29	0.0287	0.0225	0.024	0.018
31	0.0078	0.0081	0.015	0.011
33	0.053	0.053	0.047	0.047
35	0.0182	0.021	0.017	0.016
37	0.0027	0.0047	0.0026	0.0034
39	0.0035	0.0051	0.0037	0.0032
41	0.0035	0.0064	0.003	0.0013
43	0.0046	0.0083	0.0033	0.0026
45	0.0015	0.001	0.0029	0.004
47	0.005	0.003	0.004	0.0039
49	0.00285	0.002	0.001	0.001
51	0.002	0.002	0.003	0.002
53	0.0084	0.008	0.008	0.006
55	0.0151	0.01	0.015	0.014
57	0.00052	0.0008	0.001	0.0017
59	0.00826	0.0075	0.01	0.0073
61	0.0028	0.0018	0.002	0.002
63	0.0011	0.00066	0.001	0.0007
THD	**0.104015**	**0.09365**	**0.100048**	**0.076091**

Table 6 presents the results comparison of conventional and fuzzy method in terms of THD at PCC. Figure 12 shows the plot of conventional and proposed method THD results for different cases. It is proved that with the proposed method, the THD at PCC is reduced by 38%.

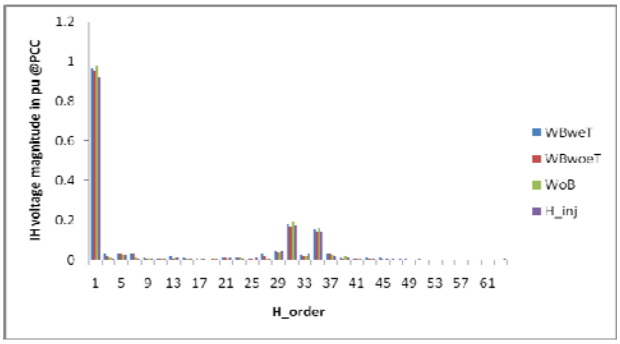

Fig. 10. Conventional method ($p = 33$) IH plot for different cases.

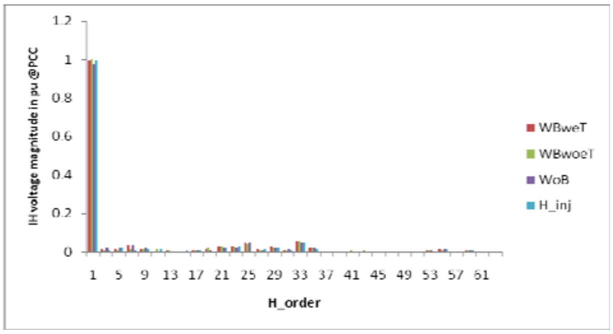

Fig. 11. Proposed fuzzy method ($p = 57$) IH plot for different cases.

Table 6. THD results comparison between conventional and proposed fuzzy method for different cases.

Different cases studied	THD in pu @ PCC	
	Conventional	Proposed fuzzy method
WBweT	0.2627	0.104015
WBwoeT	0.2487	0.09365
WoB	0.2718	0.100048
H_inj	0.2548	0.0761

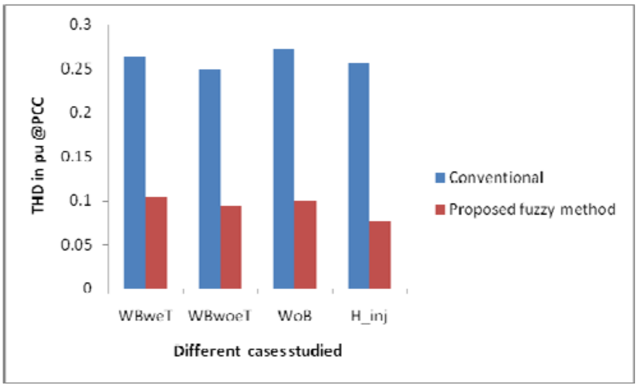

Fig. 12. Plot of conventional and proposed method THD results for different cases.

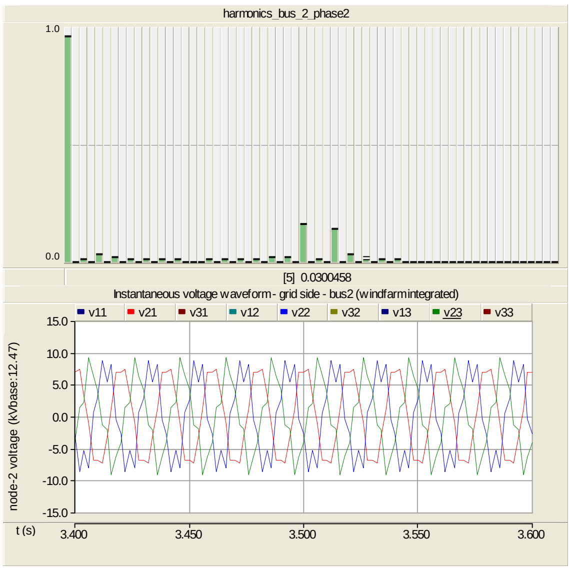

(a)

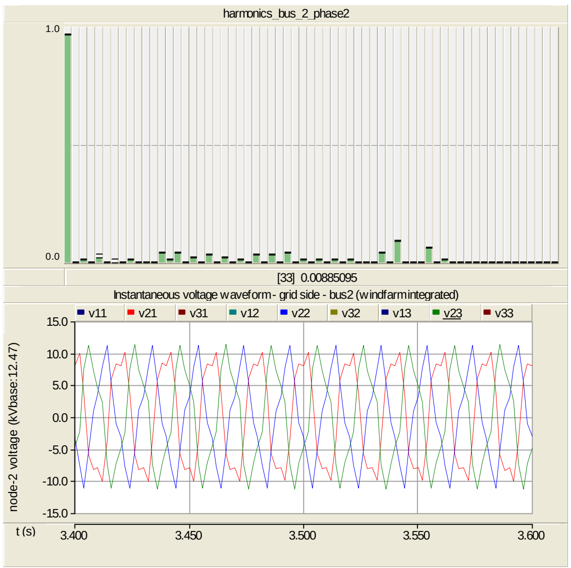

(b)

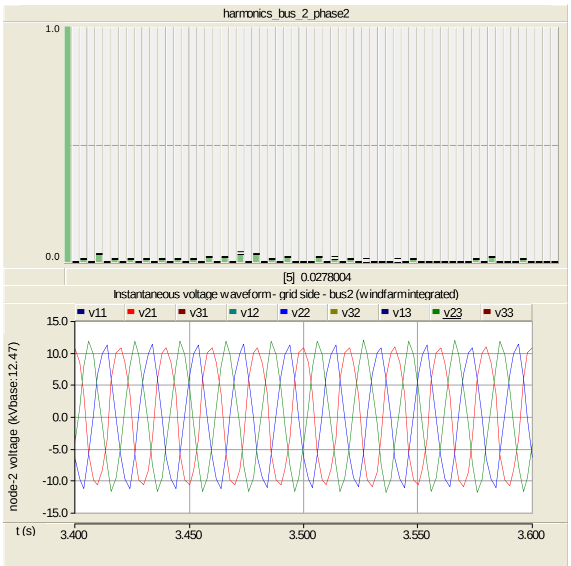

(c)

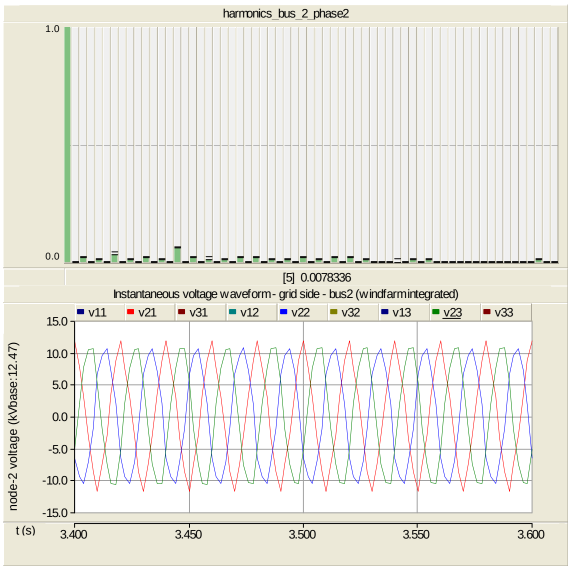

(d)

Fig. 13. Visual displays of individual harmonics and instantaneous voltage waveform at the node of interest for frequency ratios $p = (a)\,33, (b)\,57\ and\ (c)\,63$.

Figure 13 shows the visual display of the individual harmonics and the instantaneous voltage waveform at the node of interest for frequency ratios of $p = 33, 45, 57\ and\ 63$. It is evident that the individual harmonic distortion and hence the instantaneous voltage waveform distortion is very less for $p = 57$ case which is the choice of frequency ratio from numerical-fuzzy inference for PWM inverter control.

7. THE SFLA FOR OPTIMAL CHOICE OF FREQUENCY RATIO

In order to further reinforce the proposed numerical-fuzzy inference method, the Shuffled Frog Leap Algorithm (SFLA) is used to optimize the choice of frequency for a global minimum of THD.

7.1 Problem formulation

The control variable is the frequency ratio p given by (3). The objective is to minimize the THD, which is the fitness function, given by

$$F(X) = THD = \sum_{h=2}^{n}\left(\sqrt{\frac{V_h^2}{V_1^2}}\right) \quad (5)$$

In the spectral model of bipolar double-edge modulated PWM waveform using double Fourier series method given in (1), the second term is harmonics of carrier frequency which is given in (6).

$$SM_{bpdpwm}(t)_{2-term} = \sum_{m=1}^{+\infty}\frac{2}{m\pi}J_0\left(\frac{m\pi M}{2}\right)\sin\frac{m\pi}{2}\cos[m(\omega_c t + \theta_c)] \quad (6)$$

In (6), the ω_c term is replaced with the control variable p by using (3) to make the harmonics of carrier a function of the control variable.

$$i.e., \omega_c = 2\pi \times p \times f_1 \tag{7}$$

In (6), the amplitude modulation index M is chosen to be 0.9 and the initial phase angle of carrier θ_c to be zero for analysis purpose. This equation is solved for getting the individual harmonic magnitude V_h for $m = 2$ *to* 49 and the THD is computed.

7.2 SFLA specific to problem under consideration

Generate random population of P solutions (frogs). The population size is chosen as 20 and is the frequency ratios for renewable energy source PWM inverter in odd multiples of three. For each individual $i \in P$ calculate fitness(i). The fitness function is the THD given by (5). Then the population P is sorted in descending nature of their fitness.

Divide P into $'m1'$ memeplexes; the population is divided into five memeplexes, each memeplex comprising four fits. For these five memeplexes, the worst and best frogs are determined. Then the worst frog position is improved using (8 & 9) given below:

$$Change\, in\, frog\, position\, (D_i) = rand() \times (X_b - X_w) \tag{8}$$

$$New\, position\, of\, X_w = Current\, position\, of\, X_w + D_i \tag{9}$$

$$D_{\max} \geq D_i \geq -D_{\max}$$

Where $D_{\max}$ is the maximum allowed change in frogs position and *rand()* is a random number between 0 and 1. The iterations are to be repeated for specified number. In this work, the number of iterations chosen is 200. The evolved memeplexes are combined and the population P, depending on its fitness of descending order is stored. The condition for Termination = true is checked and the iterative procedure is ended.

7.3 Simulation results and discussions

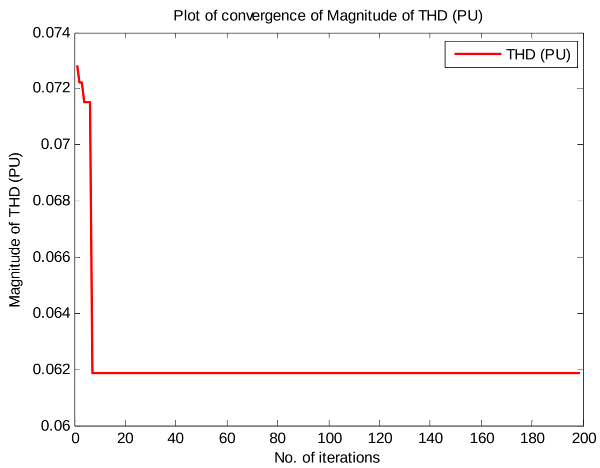

Fig. 14. Convergence characteristics for 1st run

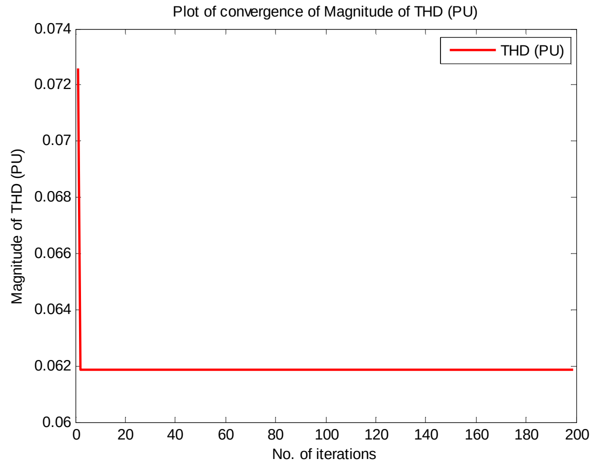

Fig. 15. Convergence characteristics for 4th run.

Table 7: The memeplexes and fits (THD) of SFLA simulation.

0.0729	**0.0619**	**0.0619**	0.0733	**0.0619**
0.0726	0.0733	0.0715	0.0733	0.0729
0.0619	**0.0619**	**0.0619**	0.0756	0.0823
0.0619	**0.0619**	**0.0619**	0.0798	**0.0619**

Table 8: The memeplexes and solutions (Frequency ratio) of SFLA simulation.

87	**57**	**57**	15	**57**
36	15	24	15	87
57	**57**	**57**	39	30
57	**57**	**57**	60	**57**

The convergence characteristics of the fits in 1st and 4th runs are shown in Figure 14 and 15 respectively. As the number of run raise, the convergence occurs earlier. The best fit is 0.0619pu THD. Table 7 and 8 presents the memeplexes of fits (THD) and solution (frequency ratio) respectively. For the best fit of 0.0619pu THD, the choice of frequency ratio is 57 as generated by SFLA.

8. REAL-TIME DIGITAL SIMULATION (RTDS) RESULTS AND DISCUSSION

In order to validate the proposed fuzzy method, the sample system (shown in Figure 1) is tested with a real-time digital simulator (RTDS). Figure 16 shows the procedure followed in RTDS validation. The host personal computer is installed with MATLAB/Simulink and OPAL-RT Technologies RT-LAB simulation software. The sample system is modeled in MATLAB/Simulink environment. RT-LAB is an open real-time GUI platform. The Simulink sample system model is loaded in RT-LAB environment. Executing the 'build' model command in RT-LAB builds real-time simulation model of the sample system. The 'execute' command executes the real-time simulation model to output RT results. It also facilitates on-line data logging, signal acquisition, signals view in scopes and parameter adjustments.

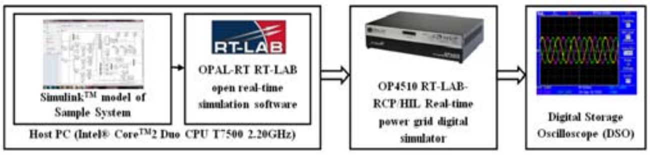

Fig. 16. Procedure followed in RTDS.

Fig. 17. RTDS using OP4150.

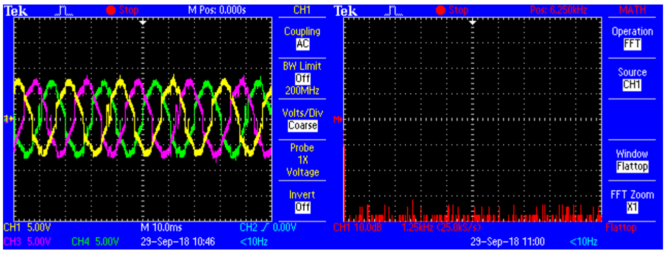

(a) p=33

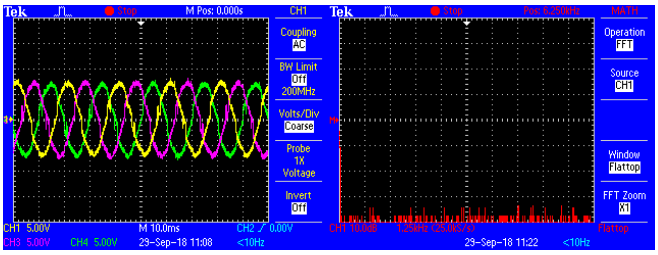

(b) p=45

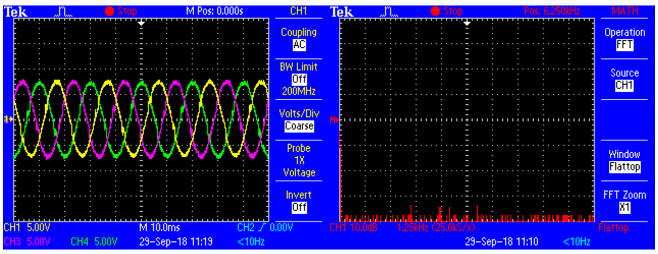

(c) p=57

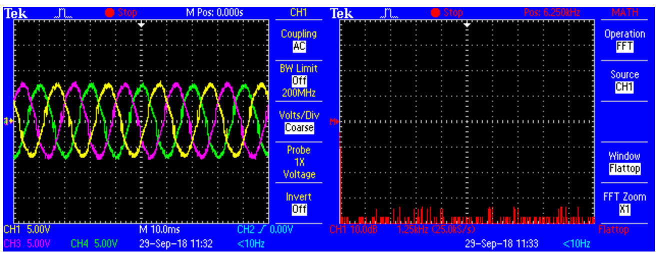

(d) p=63

Fig.18. RTDS results (PCC instantaneous voltage & IH) for inverter switching frequency ratio $p = 33, 45, 57$ and 63.

Table 9: THD at PCC comparison in different simulation environment to validate the proposed method.

Switching frequency ratios	THD at PCC (%)*		
	PSCAD/EMTDC simulation	MATLAB/ Simulink simulation	Real-time digital simulation (RTDS)
33	24.8	8.96	3.88
45	15.2	9.08	4.32
57	**10.9**	**7.72**	**2.63**
63	11.27	10.42	4.61

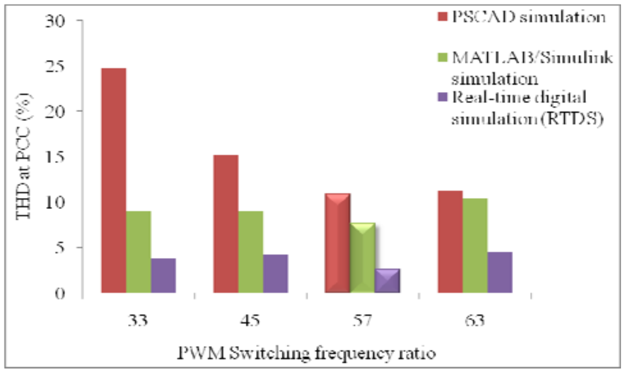

Fig. 19. THD at PCC in different simulation environments

OP4150 is OPAL-RT Technologies real-time power grid digital simulator. It integrates OPAL-RT RT-LAB with eFPGAsim real-time platform. A digital storage oscilloscope (DSO) is connected at DB37 connectors for analog outputs to visualize the instantaneous voltage profile, harmonic distortion and measure voltage magnitudes and THD at PCC where the WTG with BESS is integrated. Figure 4.21 shows the RTDS using OP4150. Figure 4.22 shows the RTDS results (PCC instantaneous voltage & IH profile) for PWM inverter switching frequencies ratio of $p = 33, 45, 57$ *and* 63. It is validated that for switching frequency ratio of $p = 57$ the instantaneous voltage profile is less distorted and the THD is 2.63%, which is the minimum as compared to the THDs 3.88%, 4.32% and 4.61% for frequency ratios of $p = 33, 45$ *and* 63 respectively. Table 9 shows the THD results comparison for different frequency ratios in PSCAD/EMTDC, MATLAB/Simulink and RTDS environments. It is evident that for the switching frequency ratio of 57 which is the output from the proposed fuzzy method, the THD is minimum for all simulation environments. Figure 19 shows the THD results comparison.

9. CONCLUSION

In this paper a numerical-fuzzy control method is proposed for choice of frequency ratio for renewable energy source PWM inverter stated by the THD and harmonic impedance scan of a radial grid. The THD and PHV are accessed at the renewable energy source integration node by varying the frequency ratio of PWM inverter. These data are the input to the numerical-fuzzy controller. The constraints imposed for choice of frequency ratio are $min(THD)$ and $min(PHV)$. The simulations are performed for various frequencies which are odd multiples of three of fundamental frequency to validate the effectiveness of the proposed methodology. For the system under consideration and its grid condition, frequency ratio of 57 fulfils both the constraints. The numerical-fuzzy controller outputs this frequency ratio for renewable energy source PWM inverter. The SFLA is applied to find an optimal frequency ratio which will provide a global minimum of THD. The outcome of SFLA is also the frequency ratio of 57. RTDS results also prove the effectiveness of the choice of frequency ratio by the proposed fuzzy method. As a future scope of work adaptive control can be implemented based on a schedule for dynamic conditions of the grid.

REFERENCES

Arricibita.D, Sanchis.P, González.R and Marroyo.L (2017). *Impedance Emulation for Voltage Harmonic Compensation in PWM Stand-Alone Inverters.* IEEE Transactions on Energy Conversion, Vol. 32, No. 4, pp. 1335-1344.

Dennis Woodford (Assessed online, 2017). *Applications of PSCAD/EMTDC*. pp. 96-97, Manitoba HVDC Research Centre Inc. Manitoba R3J 3W1, Canada.

Dghim.H, El-Naggar.A and Erlich.I (2018). *Harmonic distortion in low voltage grid with grid-connected photovoltaic.* 18th International Conference on Harmonics and Quality of Power (ICHQP), Ljubljana, pp. 1-6.

Dominguez, M, Coope, ID, Arrillaga, J and Watson, NR (1994). *An adaptive scheme for the derivation of harmonic impedance contours*. IEEE transactions on Power Delivery, Vol.9, No.2, pp.879-886.

Dommel H W (1986). *Electromagnetic Transients Program Reference Manual (EMTP Theory Book).* Bonneville Power Administration, Portland.

Geibel.D, Degner.T, Reimann.T, Engel.B, Bulo.T, Da Costa. J.P, Kruschel.W, Sahan.B, and Zacharias.P (2012). *Active intelligent distribution networks x2014; coordinated voltage regulation methods for networks with high share of decentralised generation.* In Integration of Renewable into the Distribution Grid, CIRED 2012 Workshop, pp 1–4.

Henrique L.M. Monteiro, Carlos A. Duque, Leandro R.M. Silva, Jan Meyer, Robert Stiegler, Alfredo Testa, Paulo F. Ribeiro (2017). *Harmonic impedance measurement based on short time current injections*. Electric Power Systems Research, Vol.148, pp.108–116.

Hoffmann.N, Friedrich W. Fuchs, and Asiminoaei.L (2011). *Online grid-adaptive control and active-filter functionality of pwm-converters to mitigate voltage-unbalances and voltage-harmonics - a control concept based on grid-impedance measurement.* In Energy Conversion Congress and Exposition (ECCE), 2011 IEEE, pp 3067 –3074.

Li-Xin and Jerry M.Mendal (1992). *Generating Fuzzy Rules by Learning from Examples.* IEEE Transactions on Systems, Man and Cybernetics, Vol. 22, No. 6.

Sandro Gunter, Friedrich W.Fuchs, Hans Jurgen Hinrichs (2013). *A method to measure the network harmonic impedance*. In PCIM Europe Conference, Nuremberg, pp.1666-1672.

Shankar.M and Kumudini Devi R.P (2016). *A novel generic battery modelling approach for power system simulation applications.* Journal of Advances in chemistry, Vol.12, No.6, pp.4884-4894.

Shoubaki.E et al. (2017). *Distributed µ-STATCOM for voltage support and harmonic mitigation on low voltage networks.* IEEE Applied Power Electronics Conference and Exposition (APEC), Tampa, FL, pp. 925-930.

Sun.Y, Jong. E. de, Cobben J. F. G and Cuk.V (2017). *Offshore wind farm harmonic resonance analysis — Part I: Converter harmonic model*. IEEE Manchester PowerTech, Manchester, pp. 1-6.

Task force on Harmonics Modeling and Simulation (1996a). *The modeling and simulation of the propagation of harmonics in electric power networks Part I: Concepts, models and simulation techniques*. IEEE Transactions on Power Delivery, Vol.11, No.1, pp. 452-465.

Task force on Harmonics Modeling and Simulation (1996b). *The modeling and simulation of the propagation of harmonics in electric power networks Part II: Sample systems and Examples.* IEEE Transactions on Power Delivery, Vol.11, No.1, pp. 466-474.

Tian.H, Li.Y.W and Wang.P (2018). *Hybrid AC/DC System Harmonics Control Through Grid Interfacing Converters With Low Switching Frequency.* IEEE Transactions on Industrial Electronics, Vol. 65, No. 3, pp. 2256-2267.

Vasca, F. and Iannelli, L. (2012). *Dynamics and control of switched electronic systems: Advanced perspectives for modeling, simulation and control of power converter.* pp. 25-39. Springer.

Vieto.I and Sun.J (2018). *Sequence Impedance Modelling and Converter-Grid Resonance Analysis Considering DC Bus Dynamics and Mirrored Harmonics*. IEEE 19th Workshop on Control and Modelling for Power Electronics (COMPEL), Padua, pp. 1-8.

Wang.Y, Wang.X, Blaabjerg.F and Chen.Z (2017). *Frequency scanning-based stability analysis method for grid-connected inverter system*, IEEE 3rd International Future Energy Electronics Conference and ECCE Asia (IFEEC 2017 - ECCE Asia), Kaohsiung, pp. 1575-1580.

Zou.C et al. (2018). *Analysis of Resonance between a VSC-HVDC Converter and the AC Grid*. IEEE Transactions on Power Electronics, Vol. 33, No. 12, pp.10157-10168.